High-Resolution Lead–Lag Relations Between Barents Sea Temperatures, the AMOC and the AMO During 1971–2018

Knut L. Seip & Hui Wang

View supplementary material 🗗

Published online: 11 Sep 2023.

Submit your article to this journal 🗗

View related articles 🗗

View Crossmark data 🗗

High-Resolution Lead–Lag Relations Between Barents Sea Temperatures, the AMOC and the AMO During 1971–2018

Knut L. Seip[1,*] and Hui Wang[2]

[1]*Faculty of Technology, Art and Design, Oslo Metropolitan University, Pilestredet 35, P.O. Box 4, Oslo 0130, Norway*
[2]*NOAA/NWS/NCEP/Climate Prediction Center, 5830 University Research Court, NCWCP, College Park, MD 20740, USA*

ABSTRACT   *The direction of heat transport from the atmosphere to the Barents Sea, and between the Barents Sea and the North Atlantic is important for understanding the interplay between Greenland ice melting and anthropogenic forcing. Here, we show how heat has been transported between water bodies by using a high-resolution lead-lag technique that identifies leading relations between cyclic temperature series. The results demonstrate that near-surface ocean temperature (0–30 m) in the Barents Sea led the temperature changes in its intermediate waters (100–200 m) during the period 1971 to 2018 inferring that heat transport is from the atmosphere to the intermediate waters. The Barents Sea's temperatures lagged the Atlantic meridional overturning circulation (AMOC) and the Atlantic multidecadal oscillation (AMO) from 1971 to 2000. The AMOC was leading the Barents Sea near-bottom temperatures in the West (the Bear Island Through) during 1980–2018 but was both leading and lagging in the Barents Sea Northeast.*

RÉSUMÉ   *[Trauit par la redaction] La direction du transport de chaleur de l'atmosphère vers la mer de Barents, et entre la mer de Barents et l'Atlantique Nord, est importante pour comprendre l'interaction entre la fonte des glaces du Groenland et le forçage anthropique. Nous montrons ici comment la chaleur a été transportée entre les masses d'eau en utilisant une technique de traînée à haute résolution qui détermine les relations principales entre les séries de températures cycliques. Les résultats montrent que la température de l'océan proche de la surface (0–30 m) dans la mer de Barents précède les changements de température dans ses eaux intermédiaires (100–200 m) au cours de la période 1971–2018, ce qui permet de déduire que le transport de chaleur s'effectue de l'atmosphère vers les eaux intermédiaires. Les températures de la mer de Barents sont en retard par rapport à la circulation méridienne de retournement de l'Atlantique (AMOC) et à l'oscillation multidécennale de l'Atlantique (AMO) de 1971 à 2000. L'AMOC était en avance sur les températures près du fond de la mer de Barents à l'ouest (île Bear) pendant la période 1980–2018, mais était à la fois en avance et en retard dans le nord-est de la mer de Barents.*

KEYWORDS   Barents Sea; North Atlantic; Barents Sea current variability; AMOC; AMO; NAO; lead-lag relations

1 Introduction

The objective of the present study is to examine lead-lag (LL) relations and heat transfer between the cyclic variables observed in the Barents Sea by Skagseth et al. (2020) and between Barents Sea temperature observations, the Atlantic meridional overturning circulation (AMOC) and the Atlantic multidecadal oscillation (AMO) in the North Atlantic. By identifying the LL relations between cyclic temperature series, we infer the direction of heat transport between water bodies on a decadal scale. The throughflow between

the Barents Sea and the North Atlantic is projected to increase with increasing CO_2 in the atmosphere, and with an accompanying warming of the ocean (Drinkwater et al., 2021).

a A High-Resolution Lead-Lag Method
Lead-lag relations can support interpretations of causal effects, as the cause must come before the effect. In the present context, they can help identify when an ocean mode impacts another ocean mode and for how long. The high-

resolution lead-lag (HRLL) method we use here allows us also to see, for short time windows, when LL relations are strong and when LL directions change. The shortest time window is three synoptic time steps in the paired series, and a 95% confidence interval can be identified with nine synoptic time steps. LL relations as a prerequisite for causal effects are explored in several papers (Sugihara et al., 2012; Sugihara & May, 1990; Tsonis et al., 2015). The HRLL method differs from alternative methods, e.g. cross correlation analysis (CCA), in that series do not have to be stationary. If they have a similar trend, they do not have to be detrended. The HRLL method also allows us to identify common cycle periods and phase shifts for a pair of time series (Seip et al., 2018; Seip & McNown, 2007). An important aspect of LL relations that is observed *in situ* is that they should be identified also in modelling studies.

b *The Barents Sea*
The paper does not attempt to present physical or mechanical explanations but serves as a backdrop for previous studies that discuss, and have contrasting views on, the importance of heat transports between the Barents Sea, the Labrador Sea, and the North Atlantic. The Barents Sea has been described by Skagseth et al. (2020) as a cooling machine for global warming, in the sense that the Barents Sea's warming (declining sea-ice content) will slow down its role of cooling the lower limb of the AMOC. Dickson et al. (2000) found that a high North Atlantic oscillation (NAO) index suggests an increase in the Atlantic water inflow to the Arctic Ocean via the Barents Sea Throughflow. Oldenburg et al. (2021) found that the upper ocean density in the Labrador Sea drives changes in the AMOC, whereas Li et al. (2021) showed that deep western boundary changes in the subpolar North Atlantic had minimal impact on overturning characteristics. Moore et al. (2022) showed that sea-ice retreat may cause a re-organization of water mass transformation in the Barents Sea.
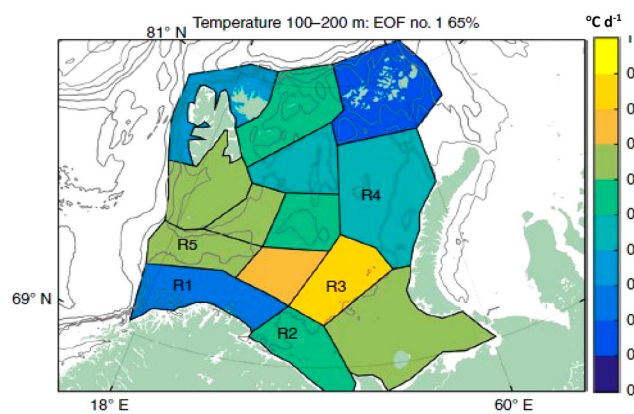

Fig. 1   The Barents Sea observation regions (Skagseth et al., 2020). Region R4 is the Barents Sea Northeast (BS-NE) and R5 is the Bear Island trough (BIT). The colour code to the right shows the amplitudes of 100–200 m temperature changes (°C d^{-1}) of the leading mode.

Contrasting views on causes and effects between ocean variabilities also exist for the North Atlantic ocean climate series, e.g. Clement et al. (2015) and Zhang et al. (2019) on AMOC and AMO. Thus, we believe that there is a need for a data-driven description of relations between ocean time series that goes beyond ordinary linear regressions (OLR) and CCA analysis.

We make three sets of analyses, the first on the LL relations between the temperature series for the upper ocean depth layer 0–30 m (UPP) and the intermediate depth layer 100–200 m (INT) in the Barents Sea. The second analysis is on the interactions between the UPP, the INT and the North Atlantic AMOC and the AMO series. The third analysis is on the interactions of near bottom flows between two Barents Sea outlets and the North Atlantic climate series, the AMOC and the AMO. For the latter two cases, we add assumptions about the validity of choosing the AMOC and the AMO as time series that interact with the Barents Sea modes.

2 Materials

The study area is the Barents Sea (18$^{\mathrm{o}}$E − 60$^{\mathrm{o}}$E, 69$^{\mathrm{o}}$N − 81$^{\mathrm{o}}$N), as shown in Fig. 1.

The hydrographic data used in the present study are from the joint Institute of Marine Research (IMR), Norway and the Nicolai M. Knipovich Polar Research Institute of Marine Fisheries and Oceanography (PINRO), Russia. We use four sets of data: (i) the observed annual temperature data for the Atlantic inflow to the Barents Sea (BS) at depths 0–30 m, UPP, and 100–200 m, INT, from 1971 to 2018; (ii) the observed annual data for temperature and salinity outflow series at the Bear Island trough (BIT) at near-bottom depths 400–420 m from 1980 to 2018; (iii) the annual temperature and salinity outflow series at the Northeast Barents Sea (BS-NE) at near-bottom depth 300–320 m from 1980 to 2018; and (iv) the observed annual data for the AMOC and the AMO from 1971 to 2018. Data (i) to (iii) were supplied by Skagseth et al. (2020) and are used to characterize temperature change and salinity flows in the Barents Sea.

Data for the AMOC was supplied by Levke Caesar, Potsdam Institute for Climate Impact Research (Caesar et al., 2021; Caesar et al., 2018). These authors reconstructed the evolution of the AMOC index based on several different and largely independent proxy indicators of the AMOC (e.g. sea surface temperatures, subsurface water mass properties and evidence for physical changes in deep – sea currents). The corroborating series cover the North Atlantic from about 40$^{\mathrm{o}}$N to 60$^{\mathrm{o}}$N (Caesar et al., 2021). Observed time series for the AMOC index are available from 2004 to 2019 (Frajka-Williams et al., 2019) and a recent version of this series was retrieved from Moat et al. (2022). A through description of the relations between the two AMOC series is given in Wang et al. (2019, pp. 1–3). The different AMOC indices show positive and negative slopes after 2007, but they also

measure different characteristics of ocean overturning circulations (Supplementary Material A). Recently, based on the trans-basin mooring array OSNAP, 2014–2018, alternative AMOC indices have been developed for the 2014–2018 period based on the thickness (m) of ocean layers delimited by density measures (kg m^{-3}). With a density-based index, Li et al. (2021) showed that events in the Labrador Sea have little impact on AMOC overturning characteristics. We choose the Caesar et al. (2021) / Moat et al. (2022) version because it covers our study period 1971 to 2018.

The time series for the unsmoothed AMO was obtained from Enfield et al. (2001), available at https://www.psl.noaa.gov/data/timeseries/AMO/ The NAO data were retrieved from https://www.ncdc.noaa.gov/teleconnections/nao/.

The AMOC series describes the volume of water transport (Sv) down to about 3500 m, the AMO describes sea surface temperatures down to approximately 5 m, and the NAO describes atmospheric surface pressure differences between a northern station, Reykjavik, and a southern station, Lisbon. The NAO index is used as a proxy for cold (-) and warm (+) phases in the North Atlantic (Dickson et al., 2000), but temperature data from Kalnay et al. (1996) on North Atlantic temperatures provides a somewhat different picture, in particular before 1995 (Supplementary Material A).

The observed series for the AMOC, the AMO and the NAO may be superpositions of several series that represent different mechanisms (Zhang et al., 2019). The LL relations between the series may therefore also depend on which of the components are examined. Attributing different mechanisms to different components in the AMO is for example shown in Fang et al. (2021).

The North Atlantic Ocean interdecadal variability shows cycle periods of about 20 years (Arzel & Huck, 2020) but also cycles with shorter and longer periods. The AMOC and the AMO both show cycle periods of 20 years (Seip et al., 2019). During the period 1971 to 2018 there was a slowdown in global warming from 1998 to 2012 (Cheng et al., 2015). Properties of the AMOC slowdown during the last bi-decade have been discussed by e.g. Boers (2021) and the impact of Arctic Sea-ice retreat by Moore et al. (2022).

Linearly detrended temperature anomaly time series normalized to unit standard deviation in the Barents Sea for both the UPP and INT layers are shown as the two lower curves in Fig. 2(a). The actual ranges of temperatures were about 3°C for the 0–30 m layer and 1–2°C for the 100–200 m layer (Skagseth et al., 2020).

3 Methods

The high-resolution LL method used here (Seip, 1997; Seip et al., 2018; Seip & McNown, 2007), and the LL method described by Krüger (2021) are to our knowledge the only LL methods that calculate LL relations over very short time windows ($n = 3$, $n = 9$ allows identification of confidence interval). They are based on a dual representation of two

time series. One is the presentation of the series along a time axis. The other is a representation in a phase diagram with one series on the x-axis and the other series on the y-axis. If the phase diagram trajectories rotate in a persistent direction, then the two series also show persistent LL relations depending upon the direction of rotation. For series normalized to unit standard deviation, the phase diagram will show an elliptic form with the major axis in the 1 : 1 or the 1 : −1 direction (Fig. 2(b,d)). A quick illustration of the relation between the two representations is given by the Lissajous curve and an example of a similar method based on synthetic series is shown in Krüger (2021).

The angle $\theta(3)$ between two sequential trajectories $\bar{v}_1$ and $\bar{v}_2$, defined by three sequential points in the phase plot, is calculated by Eq. (1).

$$\theta(3) = sign(\bar{v}_1 \times \bar{v}_2) \cdot A \cos\left(\frac{\bar{v}_1 \cdot \bar{v}_2}{|\bar{v}_1| \cdot |\bar{v}_2|}\right) \qquad (1)$$

The equation is similar to that used to describe the Coriolis force. From these angles, we identify an LL strength measure. It is formulated as a function of the number of positive angles, N_{pos}, minus the number of negative angles, N_{neg}, divided by the total numbers of positive and negative angles:

$$LL = (N_{pos} - N_{neg})/(N_{pos} + N_{neg}) \qquad (2)$$

The number $N_{tot} = N_{pos} + N_{neg} = 9$ is a trade-off between the ability to detect changes in LL relations over short time windows, and the opportunity to identify reasonably narrow confidence intervals. Since the method is relatively novel, we compare and discuss the HRLL method to traditional cross correlation analysis (CCA), e.g. as in Fang et al. (2021) and in Supplementary Material B.

Detrending and smoothing. We detrend the Barents Sea data with the linearly detrending algorithm that is among the most parsimonious detrending algorithms. However, there are concerns that detrending data would shift the time in the LL relation between paired time series relative to the LL relations they have in raw, non-detrended version. We, therefore, compare their LL relations in the raw and detrended version. To our knowledge, the HRLL method is the only method that would allow comparison of time series that are not detrended.

We LOESS smooth the two time series. The LOESS algorithm has two parameters: the fraction of the series that is used as a moving window (f) and the polynomial degree for interpolating (p). Since we always use $p = 2$, we use the terminology LOESS(f) in the text, but in the legends, we use the numbers f,2 after the acronym for the variables. LOESS smoothing and filtering time series may disentangle time series that are superpositions of different frequencies describing different physical processes and different LL relations. Here, we LOESS(0.3) smooth the series to reduce high
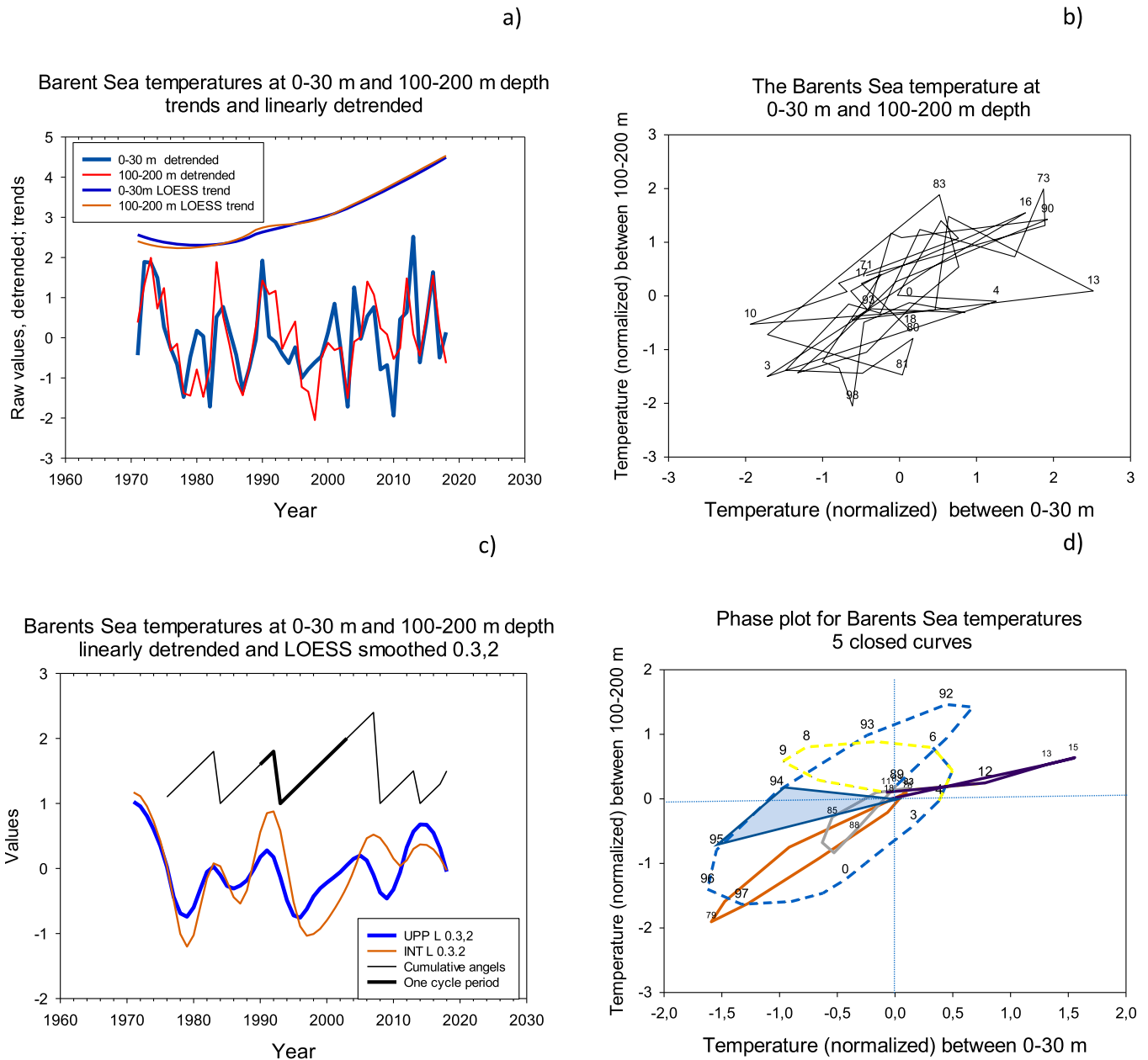
a)

Barent Sea temperatures at 0-30 m and 100-200 m depth
trends and linearly detrended

b)

The Barents Sea temperature at
0-30 m and 100-200 m depth

c)

Barents Sea temperatures at 0-30 m and 100-200 m depth
linearly detrended and LOESS smoothed 0.3,2

d)

Phase plot for Barents Sea temperatures
5 closed curves

Fig. 2   The Barents Sea temperature changes at depths 0–30 (UPP) and 100–200 m (INT). (a) The original time series from Skagseth et al. (2020) were normalized to unit standard deviation. The upper pair shows trends obtained by LOESS(0.8) smoothing the original series and shifted 3 units upward. The bottom pair shows the original series linearly detrended. LOESS smoothing is described in the text. (b) Phase diagram for the two detrended time series in (a). UPP on *x*-axis, and INT on *y*-axis. (c) Lower pair of time series in (a) LOESS(0.3) smoothed. The upper zigzag pattern shows cycle periods identified by the cumulative angle method applied to the two bottom series in Fig. 2(c) (longest cycle is 14 years). In the method section, we discuss the cumulative angle method. (d) Phase diagram of the time series in (c). Numbers are the last two digits in the year of observation. Closed curves correspond to the cycles in (c) and are colour coded separately.

frequencies that may represent noise in the series. We examine the effects of smoothing in Section 5. Discussion.

Significance. The 95% significance interval is found by applying Eq. (1) and Eq. (2) to two uniform random series. The results show that LL < –0.32 and LL > 0.32 are significant for time series longer than 9 time steps (Seip & Grøn, 2017). However, the confidence interval depends upon the characteristics of the time series, and LOESS smoothing would

increase the confidence interval. We, therefore, also consider the angle values θ(3). If the θ(3) shows persistent negative or positive values, significant LL relations are supported. Note that the θ(3) does not relate to the confidence interval.

Cycle periods. Cycle periods are calculated in three ways. First, we calculate the distance between zero crossings for the two time series normalized to unit standard deviation. Second, we apply power spectral density (PSD) algorithm

to the two time series. Cycle periods less than about 7-time steps have a probability to occur by chance that is greater than 1 : 20 for two stochastic series that interact. Third, we add cumulatively the angles, θ(3), in the phase plot for paired series. When the cumulative angle reaches 2π, one cycle is closed in the phase diagram, and this corresponds to one common cycle length for the two cyclic time series. For example, the angle, θ, is the angle with the centre in the origin and lines going out to the points numbered 94 and 95 in Fig. 2(d).

Phase shifts, or lead–lag times. If two sine series with a common cycle period, λ, coincide perfectly, the ordinary linear regression (OLR) for the cycles would show a regression coefficient = 1.0 and $r = 1.0$. If one series is displaced ¼ λ relative to the other, the two sine functions would show a perfect circle with $\beta = 0$ and $r = 0$. An approximation for the phase shift (PS) or the lead or lag time can be calculated as

$$PS = \lambda/2\pi \times (\pi/2 \pm \text{Arcsine}(r)) \qquad (3)$$

To calculate the PS, we must know the cycle period, λ, in advance.

4 Results

We first present the LL relations and the results on cycles for the Barents Sea observations UPP and INT during 1971–2018. Then we examine the LL relations between the UPP, INT, AMOC, and AMO. Last, we show the results for the temperature and salinity series for the BIT and BS-NE regions and their LL relations to the AMOC and the AMO. We only discuss the detrended series.

Both the UPP and INT waters show an increasing trend in temperature over the 1971–2018 period (Fig. 2(a)). The series are linearly detrended and LOESS(0.3) smoothed and are shown as the lower pairs of series in Fig. 2(c). Using the cumulative angle method to identify common cycle periods we obtain the cycle periods characterized by the zigzag curve in the upper part of Fig. 2(c). We identify closed curves in the phase plot, Fig. 2(d), and they show that the cycle periods for the smoothed series correspond to closed curves in the phase plot.

a *The Barents Sea Upper and Intermediate Depth Layers*
By using the HRLL method to calculate LL relations between the two temperature time series, we find that the UPP series were significantly leading the INT series until two years before the last year 2015, Fig. 3(a). Since we calculate the angles, θ(3), over three consecutive observations in the phase diagram and normalize the series to unit standard deviation, they will show an elliptic form in the 1 : 1 or 1 : −1 direction and the angles, θ(3), will typically form a wave like pattern (light grey bars) as the moving window traces the ellipsoid (Fig. 3(a)). Since the LL method examines rolling time windows for nine consecutive years, the LL

relations for the first and the last four years cannot be calculated.

b *Cycle Periods*
We used three methods to distinguish cycle periods, the zero crossing technique, the PSD method and the HRLL method.

The *zero crossings technique* showed cycle periods of 6, 6, 2, 4, 4, 11, 4, 5, 6 years for the UPP series (average 5.3 ± 2.5 years) and cycle periods of 6, 6, 2, 4, 6, 10, 10, 13 years for the INT series (average 6.7 ± 3.4 years), both series of cycle periods starting in 1971.

We apply the *PSD algorithm* to the LOESS(0.3) smoothed UPP and INT series, to the detrended AMOC series and to the AMO series, Fig. 3(b). There are common cycle periods of 7 years for the three series: UPP, INT, and AMOC. The AMO shows peaks at 4 and 8 years. However, extending the PSD graphs to longer cycle periods reveals common cycle periods of about 20 years for AMOC, AMO, and NAO (Seip et al., 2019). For the AMO series there are peaks at 4 and 8 yrs. The light blue line shows the percentage of common cycle periods that could be generated by two random series using the cumulative angle method described in the Method section. Cycle periods greater than 7 years have a probability of less than 5% to occur.

The HRLL method calculates common cycle periods for paired series with the cumulative angle method. The cumulative angle method identifies the common cycles for the two Barents Sea temperature series UPP and INT. There are four completed cycles of 8, 8, 14, and 5, giving an average of 7.6 ± 4.2 years.

c *The Barents Sea Upper and Intermediate Waters, the AMOC and the AMO*
Fig. 3(c) shows a comparison between INT and the AMOC, both LOESS(0.3) smoothed. The cycle periods found by the cumulative angle method are displayed as the see-saw line above the two time series. The AMOC is generally a leading variable to the INT (100 to 200 m) waters in the Barents Sea (Fig. 3(d)). Fig. 3(e,f) shows similar results for the UPP series (0–30 m) in the Barents Sea and the AMO. For both LL relations, the leading role of the AMOC/AMO is persistent until 1998.

d *The West Bear Island Trough and the Barents Sea-Northeast Region*
We calculate the LL relations between time series for temperature and salinity at two sub-regions, the BIT and the BS-NE and the AMOC during the period 1980 to 2018. The results are shown in Fig. 4. The AMOC is a leading variable to both temperature and salinity in the BIT region, but in the BS-NE region, the temporal relationship is more complex.

The temperature series, T (°C), and the salinity series, S (ppm), are closely associated with each other in the BIT region, but not at the BS-NE region. At the BIT region we

a)

Pos. bars: UPP (0-30 m) leads INT (100-200 m)
Neg. bars: UPP lags INT

b)

Power spectral density for climate series
UPP, 0-30m; INT, 100-200m, the AMOC, the AMO
and common cycle lengths for two random series

c)

The Barents Sea INT temperature series
and the AMOC, both LOESS smoothed

d)

Pos. bars: INT (100-200 m) leads AMOC
Neg. bars: INT(100-200 m) lags AMOC

e)

The Barents Sea UPP temperature series
and the AMO, both LOESS smoothed

f)

Pos. bars: UPP (0-30 m) leads AMO
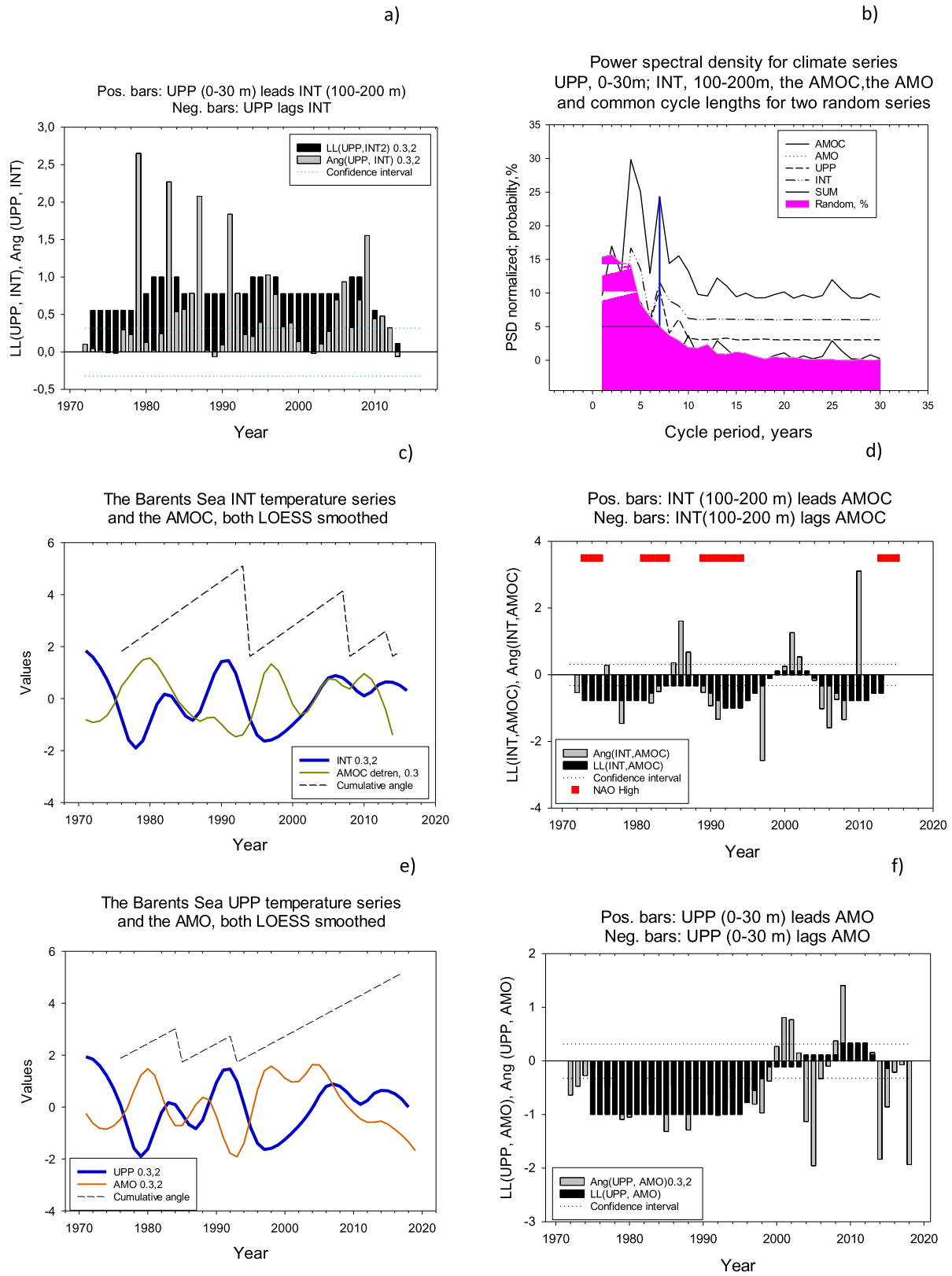Neg. bars: UPP (0-30 m) lags AMO

Fig. 3   The Barents Sea temperature changes. (a) Lead-lag relations between temperature variations in the upper ocean layer, UPP (0–30 m) and the intermediate layer, INT (100–200 m). Results are based on linearly detrended data. In the legends, the numbers f, 2 are the LOESS smoothing parameters. (b) Power spectral density for the series discussed in the text. (c) Time series for the Barents Sea INT (100–200 m) and the AMOC. (d) LL relations between the Barents Sea INT (100–200 m) and the AMOC, 1971–2018, θ(3) and LL(9). (e) Time series for the Barents Sea UPP (0–30 m) and the AMO. (f) LL relations between the Barents Sea UPP and the AMO, 1971–2018, θ(3) and LL(9). Dashed horizontal lines suggest confidence interval.
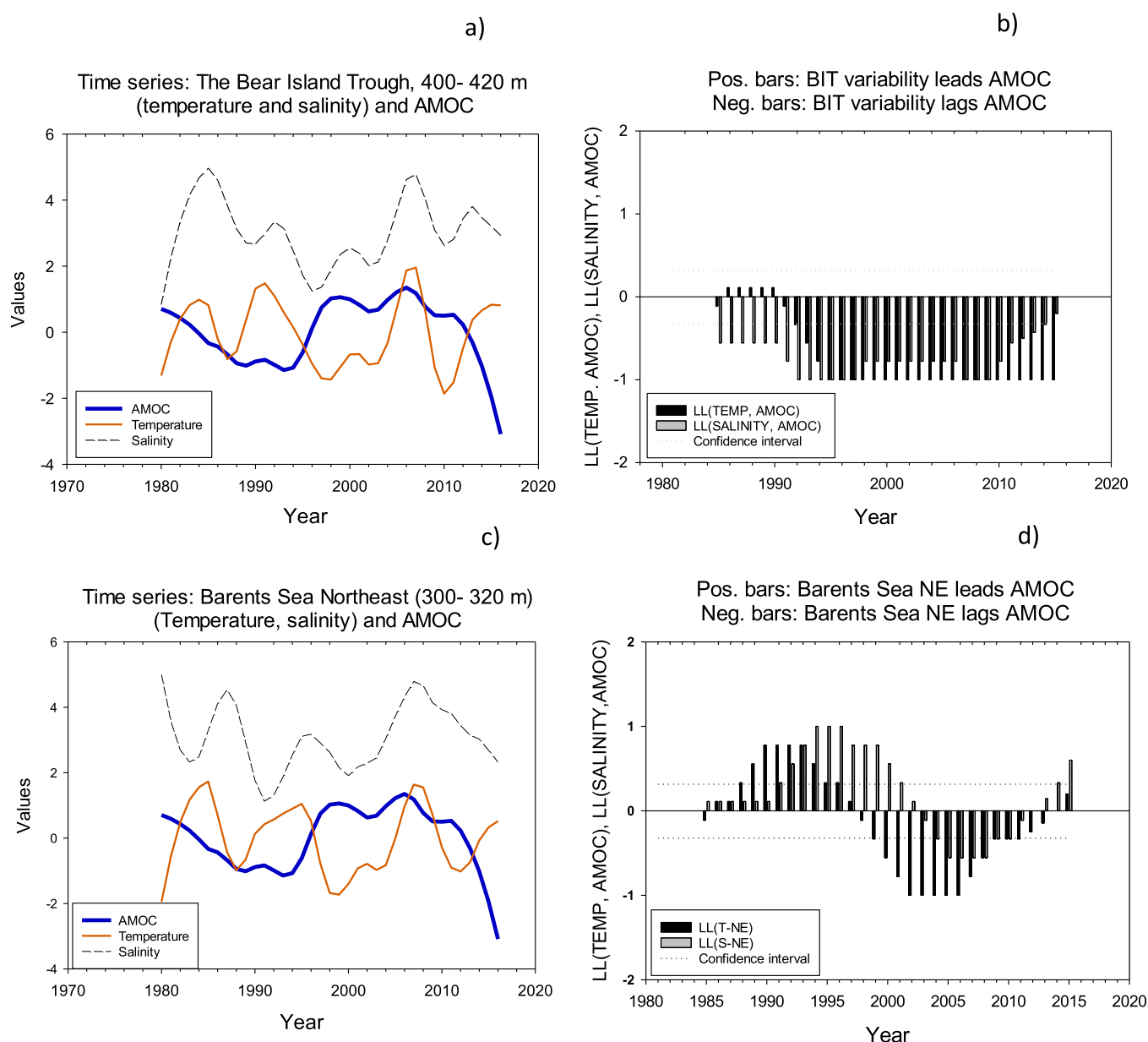
Fig. 4   Lead-lag (LL) relations between near-bottom temperature/salinity 1980–2018 at two locations in the Barents Sea and the AMOC. (a) Time series for temperature and salinity at the Bear Island Trough, BIT, south of the Bear Island for the depth range 400–420 m and for the AMOC. (b) LL relations for the two pairs of time series: Temperature vs. AMOC and salinity vs. AMOC. (c) Time series for temperature and salinity at Barents Sea Northeast, BS-NE, for the depth range 300–320 m and for the AMOC. (d) LL relations for the two pairs of time series: Temperature vs. AMOC and salinity vs. AMOC.

get $T = 2.0 \pm 0.7$ and $S = 35.01 \pm 0.04$. A regression between T and S results in $r = 0.56$, $p < 0.001$, $n = 39$.

At the BS-NE region, $T = -0.60 \pm 0.47$ and $S = 34.92 \pm 0.03$. A regression between T and S results in $r = 0.09$, $p > 0.59$, $n = 39$. We find that the AMOC was a leading variable to both the temperature and salinity series at the BIT region (Fig. 4(a,b)). However, at the BS-NE region, the AMOC was a significant lagging variable to temperature from 1991 to 1996, but a leading variable from 2000 to 2010 (Fig. 4(c, d)). The salinity series were leading series from 1991 to 2000, consistent with the AMOC as a density driven

circulation. However, salinity became a lagging series from 2004 to 2010. In the BS-NE region it appears that there could be cycles in the LL relations of 10 to 15 years. The series at both locations, when paired to the AMOC, showed only one cycle greater than 7-time steps (significant at 95% level.)

5 Discussion

We first discuss the concept of causality, cycles, and LL relations in the context of cyclic series. Then we examine

the two temperature series in the Barents Sea, INT, and UPP. Third, we discuss their relations to the AMOC and the AMO. Last, we discuss the temperature and salinity series at the near bottom at the outlet regions BIT and the BS-NE and their LL relations to the AMOC and the AMO.

a Causality, Cycle Periods and LL Relations

To show that oceanic processes may impact each other, OLR is often applied to the two-candidate series representing the processes, and the resulting explained variance, R^2, is reported. Here, we add two new measures. We examine the LL relations between the time series, and we also examine if the two series have common cycle periods. Comparing LL relations between the two Barents Sea temperature series, the raw series and the detrended and smoothed series suggest that removing noise by lightly smoothing is required, but detrending does not change LL relations much, Supplementary Material C.

When we interpret LL relations, we assume that a persistent leading relation contributes to a causal effect for the target series. However, this is not a necessary conclusion. For example, with reference to biology, one plankton species may respond more slowly to temperature than another plankton species, and thus appear to be affected by the first (Seip & Reynolds, 1995).

It is a challenge to identify a recurrent cyclic pattern in ocean variability, if it exists (Mann et al., 2020). Many studies apply types of smoothing or removal of high frequency variability from ocean temperature series. For example, Hand et al. (2020) used a 10-yr low-pass filter. There is no canonical way to determine an appropriate degree of smoothing since dynamic chaos may create unpredictable cyclic pattern (Li et al., 2020; Tomte et al., 1998). Stronger smoothing may identify sections of longer cycle periods, but the Barents Sea series are too short to establish cycle periods longer than those we identify here.

b Barents Sea Upper and the Intermediate Waters

Although heat that is generated by enhanced CO_2 concentrations in the atmosphere is small, 0.4–0.9 Wm^{-2}, about 90% of the heat flux into the oceans is stored in the oceans (Trenberth, 2020). Therefore, net heat transport during global warming would be from the atmosphere to the oceans. However, there are pauses in the warming of the globe surface that may be caused by cold waters being brought to the surface layers of the oceans (Wu et al., 2019). One of these pauses, 1998 to 2012, is within the time window studied here. Second, there may also be localized atmospheric fluctuations in the heat transport (Alexander et al., 2002) that affect the heat transport between ocean layers in the Barents Sea. Third, heat may be transported from lower latitude oceans. Lastly, the winter mixed layer in the Barents Sea may be as deep as

the intermediate layer (≈ 150 m), and, therefore, potentially affect the net heat transport between the layers. However, heat transport from third sources or enhanced mixing depth is not sufficient to break up the LL relation between UPP and INT that is shown in the time series representation and in the numerical results.

1 LEAD-LAG RELATIONS

The LL relations show that the temperature in the upper layer is a leading variable to the temperature in the lower layer. An interpretation may be that it is the changes in the atmospheric temperature that affect the temperature in the Barents Sea during the period 1971 to 2018. This is consistent with the conjecture by Skagseth et al. (2020) that there is little evidence that the upper-ocean warming is driven by increased upward mixing of heat from the warmer layer below in the northeast Barents Sea.

2 CYCLE PERIODS

The two Barents Sea time series show four equal cycle periods from the beginning of the series, 1971 to 1988. From around 2000, the two series starte to diverge in cycle periods. The year 2000 corresponds with Skagseth et al. (2020) findings that the year 2004 distinguishes a "cold" period (1985–1999) from a "warm" period (2004–2018), the latter corresponding to a warming of the near-bottom temperature, a retreating sea-ice, and a one-quarter phase lag between surface and subsurface. The cycle periods are short, and the cycles, ≈ 7 years, found by the cumulative angle method are just outside the 95% confidence interval for stochastically generated cycles, and therefore only weakly significant.

c The Barents Sea Outlets the AMOC and the AMO

There is abundant literature on possible relations between processes in the Barents Sea, the Labrador Sea, and the AMOC. However, recently there have been concerns regarding the importance of processes in the Barents Sea and the Labrador Sea for the AMOC; e.g. Li et al. (2021) on the Labrador Sea and Asbjornsen et al. (2020) on the Barents Sea. The Li et al. (2021) study covered only a short period, 2014 to 2018, but the period displayed pronounced changes in deep convection (the extended OSNAP time series were used by these authors), and, therefore, had the potential of showing effects from the Labrador Sea. However, the AMOC in density space has less variability compared to the AMOC in depth space in the subpolar region (Zhang, 2010, Fig. 2), so that a strong influence from the Labrador Sea would be less likely observed. Here, we focus on the currents at Barents Sea outlets and their interaction with AMOC (in depth space) and the AMO currents in the North Atlantic. We presently are unable to provide mechanistic arguments for which of the two AMOC versions that would be most relevant for explaining the Barents Sea observations, but AMOC in

density space is dependent on god characteristics of the deep density structure (Le Bras et al., 2023).

1 LEAD-LAG RELATIONS

Since the AMO is defined by sea surface temperatures, we compare the UPP temperatures in the Barents Sea (0–30 m) with the AMO ($\approx$ 0–5 m). The results are similar to the AMOC results, but after 1998, the LL pattern became less persistent showing a short period 2009–2012 when AMO was lagging the UPP (Fig. 3(d,f)).

We compare temperature and salinity time series for the BIT and the BS-NE regions to the AMOC (Fig. 4(a,b)). The LL pattern at the two regions shows contrasting results. In the West (BIT), the AMOC significantly leads the near-bottom temperatures from 1992 to 2014. In the Northeast, BS-NE, the AMOC leads the near bottom temperatures until 1998 and then becomes lagging in the period 2004 to 2011. Asbjornsen et al. (2020) noted that there is a steep warming trend between 1996 and 2006 (See our Fig. 4(a)) and suggested, based on a modelling study, that the warming of the open ocean domains in the northern Barents Sea during this period is due to horizontal and vertical thermal advection and diffusion. Skagseth et al. (2020) also identified a difference between the BIT and the BS-NE throughflow branches.

In the period from 1971 (the start of observations) and until about 2000, our results show that the AMOC is an overall leading variable to the variability of water temperatures in the BIT region. However, in the BS-NE region the near-bottom temperatures lead the AMOC (a period of 5 years if we only report statistically significant results), and then the AMOC becomes a leading variable for the near-bottom temperatures (a period of 6 years).

We have no firm explanations for the difference between the BIT and BS-NE regions, but there are some supporting explanations for the difference. The BS-NE waters are slightly less saline than the waters in the BIT region. Second, there may be an indirect effect of a Coriolis force that may distinguish stream flow characteristics between the two sides of fjords. It has, for example, been shown to be present in a fiord going East West in the Spitsbergen (Pawlowska et al., 2017). Normally, a Coriolis force would enhance salinity on one side of a fiord. Lastly, there may be atmospheric phenomenon related to, for example, the positive or negative phases of the NAO (Dickson et al., 2000) or changes in the North Atlantic temperature (Kalnay et al., 1996) that may affect the throughflow.

2 CYCLE PERIODS

The observed series for the AMOC, the AMO and the NAO are possibly superimposed series of components that each represents specific mechanisms (Fang et al., 2021). The mechanisms may be generated by internal processes that have their source in ocean dynamics or large-scale pressure differences, i.e. the NAO, and they may be generated by external processes, like sea-ice retreats in the Nordic and Barents Seas.

In addition, there will always be a high frequency stochastic noise component. Therefore, it may be reasonable that we find a complex relation between the Barents Sea water masses and the North Atlantic Ocean.

The PSD algorithm shows that the two temperature series from the Barents Sea, the AMOC and the AMO time series give cycle time of 7 to 9 years. To our knowledge, there is no definitive solution to the question of "true" cycles in climate series. If two mechanisms interact, peaks or troughs in the observed pattern may be the result of the interaction and not be caused by any of the two mechanisms.

Interpretations. Our interpretation of the LL relations and the cycle patterns that we observe parallels the interpretation that there are external and internal forcing processes acting on different time scale. On the decadal, medium frequency scale, Fang et al. (2021) conjecture that variabilities are due to internal mechanisms in ocean system, whereas on the multi-decadal, low frequency scale, they conjecture that variabilities are due to external forces.

The medium frequency components show the 20-year and 50-year cycles that may be internally driven and where the energy source for perturbations is baroclinic instability (Arzel & Huck, 2020; Arzel et al., 2018). However, Seip and Grøn (2019) found in a simulation study that when stochastic cycles in two adjacent ocean basins interact, they tend to show distinct cycle periods in both basins, but shift in time. Decadal cycle periods in the North Atlantic may also be related to local atmospheric processes that generate ocean circulation and changes in ocean heat transport (Hand et al., 2020). In addition to the cyclic patterns, there are LL relations between cyclic components in the AMOC, the AMO, and the NAO (Fang et al., 2021). There are different views on the direction of the LL relations, such as how they change and which frequencies the relations apply to. Fang et al. (2021) argued for the LL relation AMOC →AMO (AMV) on a decadal time scale. Nigam et al. (2020) suggested the LL relation NAO →AMO on decadal time scales. Seip and Wang (2022, Fig 7) found LL relations NAO →AMO →AMOC on decadal time scale, but not for high frequency, interannual time scales. However, low frequency oscillations, with periods longer than $\approx$ 80 years were not examined in any of the studies.

With the time span we are discussing ($\approx$ 50 years), low frequency components with multidecadal cycle periods are not possible to study numerically with sufficient confidence. Moore et al. (2022) demonstrated that there is a long-term trend, $\approx$ 50 years, in the heat flux for the Barents Sea Branch progressing from the Norwegian Sea through the Barents Sea towards the Novaya Zemlya. This heat flux may impact the low frequency component of the AMOC.

Mechanistic explanations are best formulated in modelling studies that are subsequently tested against observations and LL relations among paired variables.

In summary we find that until about 2000 the leading relation was from the UPP waters in the Barents Sea to the INT waters and the AMOC and AMO were both leading the UPP and the INT waters. However, the BIT and the BS-NE regions show

contrasting patterns. Whereas in the BIT region, the AMOC was always leading, at the BS-NE region there was a cyclic LL pattern both for temperatures and salinities. Around the year 2000, persistent patterns ceased. An interpretation for the results for the ≈ 30 years period from 1971 to 2000 would be that both atmospheric variability and variabilities caused by AMOC and AMO influence the Barents Sea variabilities. It is reasonable that the atmospheric variabilities reflect variabilities in the AMOC and that the two forces act in some type of concert to make their imprint on Barents Sea variabilities. The changing LL patterns after 2000 may be the result of the increasing role for greenhouse gas concentrations in the atmosphere since about 1880, but Klavans et al. (2022) suggested that the dominating role start after 1950.

d Robustness

The AMOC can be measured and presented in several ways. For example, Wang et al. (2019) and the version by Caesar et al. (2021) generally fit peaks and troughs in the AMOC as measured at 26.5°N (2004–2016, but not in absolute values). We chose to use the AMOC (C) series from Caesar et al. (2021) because the RAPID AMOC series from Moat et al. (2022) starts at 2004 and is, therefore, much shorter than our time period. Additionally, it is characteristic for the Atlantic Ocean south of 26°N. In Supplementary Material A, we calculate the LL relation between INT and AMOC based on an extension of AMOC (C) with the observed AMOC RAPID series from 2007, LL (INT, AMOC Ext.). The results from 2010 to 2020 suggest that INT leads AMOC, that is opposite from the AMOC (C) results for the last 10 years. However, the two series have opposite slopes after 2007. The LL(UPP, AMO) series and the LL(INT, AMOC(C)) series provide similar LL relations from 1971 to 2007, but ambiguous results after that time, supporting none of the AMOC versions, Fig. 3(d,f).

The robustness of the LL relations can be evaluated by comparing LL relations between peaks and troughs in the paired time series. In Supplementary Material B we calculate the time series for INT and AMOC(C) with two LL methods, the HRLL method used here and the CCA method where one series (here the AMOC) is shifted relative to the other. First, we apply CCA to the time window 1971–1998, where we find that INT persistently lags AMOC and we find that the regression coefficient, R, peaks at time steps –4 and +4, suggesting that there is no identifiable LL relation. However, visually inspecting the two time series, INT appears to lag AMOC with 2 to 3 years, consistent with the results from the HRLL method. Second, we apply CCA method to the whole series 1971–2021, the cross-correlation pattern is much less regular, suggesting that AMOC lags INT with more than 8 years. We conclude that the results with the HRLL method fit better to the visual LL patterns than the results from the CCA method.

An additional way to evaluate the robustness of the method is to apply the HRLL method to identical time series where one series is shifted backward in time (δ) units to mimic a causal relation between them. However, the parameter δ should be less than ½ of the series cycle period to obtain a positive LL relation, Supplementary Material D.

There are four additional important caveats in the interpretation of the LL results. The time series we discuss are short (≈ 40 years) and the LL relations between temperature variabilities among ocean basins may change on a interdecadal time scale (Seip et al., 2019). Therefore, our results may not apply to heat fluxes between the North Atlantic and the Barents Sea on multidecadal or centennial time scales. Second, we chose LOESS(0.3) smoothing to avoid high frequency variability, but smoothing might distort the series. There appears to be variabilities in the series with long cycle periods, for example, 60–80 years for the AMOC (Arzel & Huck, 2020; Cheng et al., 2013), but those long periods may be due to other mechanisms than those responsible for decadal variability. Third, the deep water observations are down to 200 m (≈ 400 m being close to bottom temperatures), but the relevant depths for the AMOC variability is down to 3500 m (Perez et al., 2015; Wang et al., 2019). However, the AMOC and the AMO covary (R ≈ 0.5) result in roughly the same LL relations. Furthermore, the exact pathways and properties of the deep waters entering the North Atlantic from the Nordic Seas/Barents Sea/Arctic are strongly influenced by the complex bottom topography, including ridges (Hand et al., 2020), and our results suggest that bottom topography, as well as the Coriolis force, may be candidates for explaining the difference between the BIT and the BS-NE regions. Lastly, we could have lengthened the period of nine time steps for calculating the moving LL window, but preferred the nine time intervals to be able to detect rapid changes in LL relations.

6 Conclusion

Applying the high-resolution method for identifying lead-lag relations between paired time series, we find that the upper ocean temperatures (0–30 m) in the Barents Sea from 1971 to 2018 were leading temperature changes in intermediate waters (100–200 m). We find that both the AMOC and the AMO were a leading variable to the temperature series in the Barents Sea at 100 to 200 m depth during the period 1971 to 2018 and at the Bear Island trough 400–420 m during the period 1980 to 2018. In contrast, the AMOC was both a leading and a lagging series to temperature and salinity in the BS-NE region.

Our results support the view that, at least over the most recent 30 years from 1971 to 2000, it is the AMOC and the AMO that influence the Arctic waters, but there are important exceptions after the year 2000 for the AMO (Fig. 3(f)) and for the AMOC in Northeast Barents Sea throughout the full period (Fig. 4(b)). We suggest that different mechanisms on decadal and multidecadal time scales drive the interactions between the Barents Sea and the North Atlantic currents. On decadal time scales, 10–30 years, internal mechanisms in the North

Atlantic currents AMO and AMOC determine cycle periods and LL relations. On multidecadal time scale, external forces that affect the Barents Sea drive the interactions.

Disclosure statement

No potential conflict of interest was reported by the author(s).

Supplemental data

Supplemental data for this article can be accessed online at https://doi.org/10.1080/07055900.2023.2251426.

Data availability statement

All data and all calculations are available from the first author. Essential calculations and figures are made in a spreadsheet (Excel) and an example is shown in word format in Supplementary Material C. Some auxiliary calculations and the final figures are made in SigmaPlot. However, all calculations could be made in most computer packages.

References

Alexander, M. A., Blade, I., Newman, M., Lanzante, J. R., Lau, N. C., & Scott, J. D. (2002). The atmospheric bridge: The influence of ENSO teleconnections on air-sea interaction over the global oceans. *Journal of Climate*, *15*(16), 2205–2231. https://doi.org/10.1175/1520-0442(2002)015<2205:Tabtio>2.0.Co;2

Arzel, O., & Huck, T. (2020). Contributions of atmospheric stochastic forcing and intrinsic ocean modes to North Atlantic Ocean interdecadal variability. *Journal of Climate*, *33*(6), 2351–2370. https://doi.org/10.1175/Jcli-D-19-0522.1

Arzel, O., Huck, T., & de Verdiere, A. C. (2018). The internal generation of the Atlantic Ocean interdecadal variability. *Journal of Climate*, *31*(16), 6411–6432. https://doi.org/10.1175/Jcli-D-17-0884.1

Asbjornsen, H., Arthun, M., Skagseth, O., & Eldevik, T. (2020). Mechanisms underlying recent Arctic Atlantification. *Geophysical Research Letters*, *47*(15). https://doi.org/10.1029/2020GL088036

Boers, N. (2021). Observation based early warning signals for a collapse of the Atlantic meridional overturning circulation. *Nature Climate Change*, *11*(8), 680–688. https://doi.org/10.1038/s41558-021-01097-4

Caesar, L., McCarthy, G. D., Thornalley, D. J. R., Cahill, N., & Rahmstorf, S. (2021). Current Atlantic meridional overturning circulation weakest in last millennium. *Nature Geoscience*, *14*(3), 118–120. https://doi.org/10.1038/s41561-021-00699-z

Caesar, L., Rahmstorf, S., Robinson, A., Feulner, G., & Saba, V. (2018). Observed fingerprints of weakening Atlantic Ocean overturning circulation. *Nature*, *556*(7700), 191–196. https://doi.org/10.1038/s41586-018-0006-5

Cheng, L. J., Zheng, F., & Zhu, J. (2015). Distinctive ocean interior changes during the recent warming slowdown. *Scientific Reports*, *5*. https://doi.org/10.1038/srep14346

Cheng, W., Chiang, J. C. H., & Zhang, D. X. (2013). Atlantic meridional overturning circulation (AMOC) in CMIP5 models: RCP and historical simulations. *Journal of Climate*, *26*(18), 7187–7197. https://doi.org/10.1175/Jcli-D-12-00496.1

Clement, A., Bellomo, K., Murphy, L. N., Cane, M. A., Mauritsen, T., Radel, G., & Stevens, B. (2015). The Atlantic multidecadal oscillation without a role for ocean circulation. *Science*, *350*(6258), 320. https://doi.org/10.1126/science.aab3980

Dickson, R. R., Osborn, T. J., Hurrell, J. W., Meincke, J., Blindheim, J., Adlandsvik, B., Vinje, T., Alekseev, G., & Maslowski, W. (2000). The Arctic Ocean response to the North Atlantic oscillation. *Journal of Climate*, *13*(15), 2671–2696. https://doi.org/10.1175/1520-0442(2000)013<2671:Taortt>2.0.Co;2

Drinkwater, K. F., Harada, N., Nishino, S., Chierici, M., Danielson, S. L., Ingvaldsen, R. B., Kristiansen, T., Hunt, G. L., Mueter, F., Stiansen, J. E., & Anderson, E. (2021). Possible future scenarios for two major Arctic gateways connecting subarctic and Arctic marine systems: I. Climate and physical-chemical oceanography. *ICES Journal of Marine Science*, *78*(9), 3046–3065. https://doi.org/10.1093/icesjms/fsab182

Enfield, D. B., Mestas-Nunez, A. M., & Trimble, P. J. (2001). The Atlantic multidecadal oscillation and its relation to rainfall and river flows in the continental US. *Geophysical Research Letters*, *28*(10), 2077–2080. https://doi.org/10.1029/2000gl012745

Fang, S. W., Khodri, M., Timmreck, C., Zanchettin, D., & Jungclaus, J. (2021). Disentangling internal and external contributions to Atlantic multidecadal variability over the past millennium. *Geophysical Research Letters*, *48*(23), e2021GL095990. https://doi.org/10.1029/2021GL095990

Frajka-Williams, E., Ansorge, I. J., Baehr, J., Bryden, H. L., Chidichimo, M. P., Cunningham, S. A., Danabasoglu, G., Dong, S. F., Donohue, K. A., Elipot, S., Heimbach, P., Holliday, N. P., Hummels, R., Jackson, L. C., Karstensen, J., Lankhorst, M., Le Bras, I. A., Lozier, M. S., McDonagh, E. L., … Wilson, C. (2019). Atlantic meridional overturning circulation: Observed transport and variability. *Frontiers in Marine Science*, *6*. https://doi.org/10.3389/fmars.2019.00260

Hand, R., Bader, J., Matei, D., Ghosh, R., & Jungclaus, J. H. (2020). Changes of decadal SST variations in the subpolar North Atlantic under strong CO_2 forcing as an indicator for the ocean circulation's contribution to Atlantic multidecadal variability. *Journal of Climate*, *33*(8), 3213–3228. https://doi.org/10.1175/Jcli-D-18-0739.1

Kalnay, E., Kanamitsu, M., Kistler, R., Collins, W., & Deaven, D. (1996). The NCEP/NCAR 40-year reanalysis project. *Bulletin of the American Meteorological Society*, *77*(3), 437–472. https://doi.org/10.1175/1520-0477(1996)077<0437:TNYRP>2.0.CO;2

Klavans, J. M., Clement, A. C., Cane, M. A., & Murphy, L. N. (2022). The evolving role of external forcing in North Atlantic SST variability over the last millennium. *Journal of Climate*, *35*(9), 2741–2754. https://doi.org/10.1175/JCLI-D-21-0338.1

Krüger, J. J. (2021). A wavelet evaluation of some leading business cycle indicators for the German economy. *Journal of Business Cycle Research*, *17*(3), 293–319. https://doi.org/10.1007/s41549-021-00060-8

Le Bras, I. A. A., Willis, J., & Fenty, I. (2023). The Atlantic meridional overturning circulation at 35 degrees N from deep moorings, floats, and satellite altimeter. *Geophysical Research Letters*, *50*(10). https://doi.org/10.1029/2022GL101931

Li, F., Lozier, M. S., Bacon, S., Bower, A. S., Cunningham, S. A., de Jong, M. F., de Young, B., Fraser, N., Fried, N., Han, G., Holliday, N. P., Holte, J., Houpert, L., Inall, M. E., Johns, W. E., Jones, S., Johnson, C., Karstensen, J., Le Bras, I. A., … Zhou, C. (2021). Author correction: Subpolar North Atlantic western boundary density anomalies and the meridional overturning circulation (vol 12, 3002, 2021). *Nature Communications*, *13*(1). https://doi.org/10.1038/s41467-022-28397-3

Li, F., Lozier, M. S., Bacon, S., Bower, A. S., Cunningham, S. A., de Jong, M. F., DeYoung, B., Fraser, N., Fried, N., Han, G., Holliday, N. P., Holte, J., Houpert, L., Inall, M. E., Johns, W. E., Jones, S., Johnson, C., Karstensen, J., Le Bras, I. A., … Zhou, C. (2021). Subpolar North Atlantic western boundary density anomalies and the meridional overturning circulation. *Nature Communications*, *12*(1). https://doi.org/10.1038/s41467-021-23350-2

Li, S. J., Wu, L. X., Yang, Y., Geng, T., Cai, W. J., Gan, B. L., Chen, Z. H., Jing, Z., Wang, G. J., & Ma, X. H. (2020). The Pacific decadal oscillation less predictable under greenhouse warming. *Nature Climate Change*, *10*(1), 30. https://doi.org/10.1038/s41558-019-0663-x

Mann, M. E., Steinman, B. A., & Miller, S. K. (2020). Absence of internal multidecadal and interdecadal oscillations in climate model simulations. *Nature Communications*, *11*(49). https://doi.org/10.1038/s41467-019-13823-w. www.nature.com/naturecommunications

Moat, B. I., Frajka-Williams, E., Smeed, D. A., Rayner, D., Johns, W. E., Baringer, M. O., Volkov, D., & Collins, J. M. (2022). *Atlantic meridional overturning circulation observed by the RAPID-MOCHA-WBTS (RAPID-meridional overturning circulation and heatflux array-western boundary time series) array at 26N from 2004 to* 2020. https://doi.org/10.5285/e91b10af-6f0a-7fa7-e053-6c86abc05a09. https://rapid.ac.uk/rapidmoc/rapid_data/datadl.php

Moore, G. W. K., Våge, K., Renfrew, I. A., & Pickart, R. S. (2022). Sea-ice retreat suggests re-organization of water mass transformation in the Nordic and Barents seas. *Nature Communications*, *13*(1), 67. https://doi.org/10.1038/s41467-021-27641-6

Nigam, S., Sengupta, A., & Ruiz-Barradas, A. (2020). Atlantic-Pacific links in observed multidecadal SST variability: Is the Atlantic multidecadal oscillation's phase reversal orchestrated by the Pacific decadal oscillation? *Journal of Climate*, *33*(13), 5479–5505. https://doi.org/10.1175/Jcli-D-19-0880.1

Oldenburg, D., Wills, R. C. J., Armour, K. C., Thompson, L., & Jackson, L. C. (2021). Mechanisms of low-frequency variability in North Atlantic Ocean heat transport and AMOC. *Journal of Climate*, *34*(12), 4733–4755. https://doi.org/10.1175/Jcli-D-20-0614.1

Pawlowska, J., Zajaczkowski, M., Szczucinski, W., Zaborska, A., Kucharska, M., Jernas, P. E., & Forwick, M. (2017). The influence of Coriolis force driven water circulation on the palaeoenvironment of Hornsund (S spitsbergen) over the last century. *Boreas*, *46*(4), 737–749. https://doi.org/10.1111/bor.12249

Perez, R. C., Baringer, M. O., Dong, S. F., Garzoli, S. L., Goes, M., Goni, G. J., Lumpkin, R., Meinen, C. S., Msadek, R., & Rivero, U. (2015). Measuring the Atlantic meridional overturning circulation. *Marine Technology Society Journal*, *49*(2), 167–177. https://doi.org/10.4031/Mtsj.49.2.14

Seip, K. L. (1997). Defining and measuring species interactions in aquatic ecosystems. *Canadian Journal of Fisheries and Aquatic Sciences*, *54*(7), 1513–1519. https://doi.org/10.1139/f97-058

Seip, K. L., & Grøn, Ø. (2017). A new method for identifying possible causal relationships between CO2, total solar irradiance and global temperature change. *Theoretical and Applied Climatology*, *127*(3–4), 923–938. https://doi.org/10.1007/s00704-015-1675-8

Seip, K. L., & Grøn, Ø. (2019). On the statistical nature of distinct cycles in global warming variables. *Climate Dynamics*, *52*(12), 7329–7337. https://doi.org/10.1007/s00382-016-3508-6

Seip, K. L., Gron, O., & Wang, H. (2018). Carbon dioxide precedes temperature change during short-term pauses in multi-millennial palaeoclimate records. *Palaeogeography, Palaeoclimatology, Palaeoecology*, *506*, 101–111. https://doi.org/10.1016/j.palaeo.2018.06.021

Seip, K. L., Gron, O., & Wang, H. (2019). The North Atlantic oscillations: Cycle times for the NAO, the AMO and the AMOC. *Climate*, *7*(3). https://doi.org/10.3390/cli7030043

Seip, K. L., & McNown, R. (2007). The timing and accuracy of leading and lagging business cycle indicators: A new approach. *International Journal of Forecasting*, *22*(2), 277–287. https://doi.org/10.1016/j.ijforecast.2006.11.001

Seip, K. L., & Reynolds, C. S. (1995). Phytoplankton functional attributes along trophic gradient and season. *Limnology and Oceanography*, *40*(3), 589–597. https://doi.org/10.4319/lo.1995.40.3.0589

Seip, K. L., & Wang, H. (2022). The North Atlantic oscillations: Lead–lag relations for the NAO, the AMO, and the AMOC – a high-resolution lead–lag analysis. *Climate*, *10*(5), 63. https://doi.org/10.3390/cli10050063

Skagseth, O., Eldevik, T., Arthun, M., Asbjornsen, H., Lien, V. D. S., & Smedsrud, L. H. (2020). Reduced efficiency of the Barents Sea cooling machine. *Nature Climate Change*, *10*(7), 661. https://doi.org/10.1038/s41558-020-0772-6

Sugihara, G., & May, R. M. (1990). Nonlinear forecasting as a way of distinguishing chaos from measurement errors in time series. *Nature*, *344*(6268), 734–741. https://doi.org/10.1038/344734a0

Sugihara, G., May, R., Ye, H., Hsieh, C. H., Deyle, E., Fogarty, M., & Munch, S. (2012). Detecting causality in complex ecosystems. *Science*, *338*(6106), 496–500. https://doi.org/10.1126/science.1227079

Tomte, O. T., Seip, K. L., & Christophersen, N. (1998). Evidence that loss in predictability increases with weakening of (metabolic) links to physical forcing functions in aquatic ecosystems. *Oikos*, *82*(2), 325–332. https://doi.org/10.2307/3546973

Trenberth, K. E. (2020). Understanding climate change through earth's energy flows. *Journal of the Royal Society of New Zealand*, *50*(2), 331–347. https://doi.org/10.1080/03036758.2020.1741404

Tsonis, A. A., Deyle, E. R., May, R. M., Sugihara, G., Swanson, K., Verbeten, J. D., & Wang, G. L. (2015). Dynamical evidence for causality between galactic cosmic rays and interannual variation in global temperature. *Proceedings of the National Academy of Sciences of the United States of America*, *112*(11), 3253–3256. https://doi.org/10.1073/pnas.1420291112

Wang, Z. L., Brickman, D., & Greenan, B. J. W. (2019). Characteristic evolution of the Atlantic meridional overturning circulation from 1990 to 2015: An eddy-resolving ocean model study. *Deep-Sea Research Part I-Oceanographic Research Papers*, *149*. https://doi.org/10.1016/j.dsr.2019.06.002

Wu, T. W., Hu, A. X., Gao, F., Zhang, J., & Meehl, G. A. (2019). New insights into natural variability and anthropogenic forcing of global/regional climate evolution. *NPJ Climate and Atmospheric Science*, *2*. https://doi.org/10.1038/s41612-019-0075-7

Zhang, R. (2010). Latitudinal dependence of Atlantic meridional overturning circulation (AMOC) variations. *Geophysical Research Letters*, *37*. https://doi.org/10.1029/2010gl044474

Zhang, R., Sutton, R., Danabasoglu, G., Kwon, Y. O., Marsh, R., Yeager, S. G., Amrhein, D. E., & Little, C. M. (2019). A review of the role of the Atlantic meridional overturning circulation in Atlantic multidecadal variability and associated climate impacts. *Reviews of Geophysics*, *57*(2), 316–375. https://doi.org/10.1029/2019rg000644